Ultrasonics Sonochemistry 22 (2015) 41–50

Contents lists available at ScienceDirect

Ultrasonics Sonochemistry

journal homepage: www.elsevier.com/locate/ultson

Sensitivity of free radicals production in acoustically driven bubble to the ultrasonic frequency and nature of dissolved gases

Slimane Merouani [a,b,*], Oualid Hamdaoui [a], Yacine Rezgui [c], Miloud Guemini [c]

[a] Laboratory of Environmental Engineering, Department of Process Engineering, Faculty of Engineering, Badji Mokhtar – Annaba University, P.O. Box 12, 23000 Annaba, Algeria
[b] Department of Chemical Engineering, Faculty of Pharmaceutical Engineering Process, University of Constantine 3, 25000 Constantine, Algeria
[c] Laboratory of Applied Chemistry and Materials Technology, University of Oum El-Bouaghi, P.O. Box 358, 04000 Oum El Bouaghi, Algeria

ARTICLE INFO

Article history:
Received 26 April 2014
Received in revised form 16 July 2014
Accepted 16 July 2014
Available online 25 July 2014

Keywords:
Single-bubble sonochemistry
Computer simulations
Ultrasonic frequency
Saturating gas
·OH radical

ABSTRACT

Central events of ultrasonic action are the bubbles of cavitation that can be considered as powered microreactors within which high-energy chemistry occurs. This work presents the results of a comprehensive numerical assessment of frequency and saturating gases effects on single bubble sonochemistry. Computer simulations of chemical reactions occurring inside a bubble oscillating in liquid water irradiated by an ultrasonic wave have been performed for a wide range of ultrasonic frequencies (213–1100 kHz) under different saturating gases (O_2, air, N_2 and H_2). For O_2 and H_2 bubbles, reactions mechanism consisting in 25 reversible chemical reactions were proposed for studying the internal bubble-chemistry whereas 73 reversible reactions were taken into account for air and N_2 bubbles. The numerical simulations have indicated that radicals such as ·OH, H·, HO_2· and O are created in the bubble during the strong collapse. In all cases, hydroxyl radical (·OH) is the main oxidant created in the bubble. The production rate of the oxidants decreases as the driving ultrasonic frequency increases. The production rate of ·OH radical followed the order O_2 > air > N_2 > H_2 and the order becomes more remarkable at higher ultrasonic frequencies. The effect of ultrasonic frequency on single bubble sonochemistry was attributed to its significant impact on the cavitation process whereas the effects of gases were attributed to the nature of the chemistry produced in the bubble at the strong collapse. It was concluded that, in addition to the gas solubility, the nature of the internal bubble chemistry is another parameter of a paramount importance that controls the overall sonochemical activity in aqueous solutions.

1. Introduction

The chemical effects of ultrasound (sonochemistry) originate from acoustic cavitation, that is, ultrasound-induced formation, growth and violent collapse of microbubbles in a liquid medium [1]. The rapid collapse of cavitation bubbles is nearly adiabatic, rendering each individual bubble a microreactor, inside which temperatures of the order of 5000 K and pressures of hundreds of atmospheres have been shown to exist [2,3]. As a results, water vapor entrapped inside a bubble is dissociated into H· and ·OH radicals, and with other species present, various other reactive species such as HO_2·, O and H_2O_2 may form [4]. Parallel reaction pathways exist where volatile solutes may evaporate into the bubble and be pyrolysed by the high core temperatures [4]. The radical species produced can recombine, react with other gaseous species present in the cavity or diffuse out of the bubble into the surrounding liquid to serve as oxidants [5]. All chemical reactions promoted by ultrasound are known as sonochemical reactions. Under certain conditions, bubble collapse is also accompanied by the emission of light, called sonoluminescence, originating from the hot core of the bubble during the final stages of collapse [6,7].

A number of factors influence sonochemical activity (radicals' production) and luminescence intensity. These include frequency of ultrasound, dissolved gas, acoustic power, bulk liquid temperature, etc. [8–17]. Among all these parameters, the ultrasonic frequency and the nature of the dissolved gases have shown spectacular effects. The frequency of ultrasound has a significant impact on the critical size of the bubble (resonance size), which decreases as ultrasound frequency increases [18,19] and the lower frequency ultrasound would produce more violent collapse leading to higher localized temperatures and pressures in the bubble. However, recent published papers [8–10,14,15] have suggest a higher sonochemical activity at higher frequency. As a general idea,

* Corresponding author at: Department of Chemical Engineering, Faculty of Pharmaceutical Engineering Process, University of Constantine 3, 25000 Constantine, Algeria. Tel./fax: +213 (0)38876560.
E-mail address: s.merouani@yahoo.fr (S. Merouani).

http://dx.doi.org/10.1016/j.ultsonch.2014.07.011
1350-4177/

Nomenclature

A_f (A_r)	pre-exponential factor of the forward (reverse) reaction, [($cm^3\ mol^{-1}\ s^{-1}$) for two body reaction and ($cm^6\ mol^{-2}\ s^{-1}$) for three body reaction]
b_f (b_r)	temperature exponent of the forward (reverse) reaction
c	speed of sound in the liquid medium, ($m\ s^{-1}$)
E_{af} (E_{ar})	activation energy of the forward (reverse) reaction ($cal\ mol^{-1}$)
f	frequency of ultrasonic wave (Hz)
I_a	acoustic intensity of ultrasonic irradiation ($W\ m^{-2}$)
k_{f9} (k_r)	forward (reverse) reaction constant, [($cm^3\ mol^{-1}\ s^{-1}$) for two body reaction and ($cm^6\ mol^{-2}\ s^{-1}$) for three body reaction]
p	pressure inside a bubble (Pa)
p_{max}	maximum pressure inside a bubble (Pa)
p_∞	ambient static pressure (Pa)
P_A	amplitude of the acoustic pressure (Pa)
P_v	vapor pressure of water (Pa)
P_{g0}	initial gas pressure (Pa)
R	radius of the bubble (m)
R_{max}	maximum radius of the bubble (m)
R_0	ambient bubble radius (m)
t	time (s)
T	temperature inside a bubble (K)
T_{max}	maximum temperature inside a bubble (K)
T_∞	bulk liquid temperature (K)
x_i	solubility (in mole fraction) of the gas i in water
y_{H_2O}	mole fraction of water vapor trapped at the collapse

Greek letters

γ	specific heat ratio (c_p/c_v) of the gas mixture
σ	surface tension of liquid water ($N\ m^{-1}$)
ρ	density of liquid water ($kg\ m^{-3}$)
λ	gas thermal conductivity ($W\ m^{-2}\ K$)
τ_c	collapse time of the bubble (s)
τ_{exp}	expansion time of the bubble (s)

a gas with high polytropic index ($\gamma = c_p/c_v$) and low thermal conductivity converts more energy upon collapse and gives a greater sonochemical effect than one with low polytropic index. However, recent investigations [12–14,16,17] showed that polyatomic gases can provide a more sonochemical activity than monatomic gases because gases such as oxygen can provide additional sources for the production of active species through the self thermal dissociation inside a bubble and, thus, can compensate for the lower internal cavitation temperatures. On the other hand, Okitsu et al. [20] showed experimental evidence that the bubble temperature induced by high frequency ultrasound is almost the same among different gases and the overall chemical efficiency is in proportion to the gas solubility, which would be closely related to the number of active bubbles. Therefore, the mechanism of saturating gases and ultrasound frequency on the sonochemical activity remained poorly understood. This is in fact because the effects of these two parameters are not well established in microscopic scale (scale of single bubble). In this paper, the results of a comprehensive numerical assessment of frequency and saturating gases effects on sonochemical activity of single cavitation bubble were described. The numerical simulations of the bubble oscillation and chemical reactions therein have been performed for various ultrasonic frequencies (in the range of 213–1100 kHz) under different saturating gases (O_2, air, N_2 and H_2). The employed model combines the dynamic of bubble collapse in acoustic field with the chemical kinetics of single cavitating bubble.

2. Model and computational methods

The theoretical model used in the present numerical simulations has been fully described in our previous works [21–24]. The following is a brief description of the model.

2.1. Bubble dynamics model

A gas and vapor filled spherical bubble isolated in water oscillates under the action of a sinusoidal sound wave. The temperature and pressure in the bubble are assumed spatially uniform and the gas content of the bubble behaves as an ideal gas [25]. The radial dynamics of the bubble is described by the Keller–Miksis equation that includes first order terms in the Mach number $M = \dot{R}/c$ [26,27]:

$$\left(1-\frac{\dot{R}}{c}\right)R\ddot{R}+\frac{3}{2}\left(1-\frac{\dot{R}}{3c}\right)\dot{R}^2=\frac{1}{\rho_L}\left(1+\frac{\dot{R}}{c}\right)\left[p-p_\infty-\frac{2\sigma}{R}-4\mu\frac{\dot{R}}{R}+P_A\sin(2\pi ft)\right]+\frac{R}{\rho_L c}\frac{d}{dt}\left[p-p_\infty-\frac{2\sigma}{R}-4\mu\frac{\dot{R}}{R}+P_A\sin(2\pi ft)\right] \quad (1)$$

in this equation dots denote time derivatives (d/dt), R is the radius of the bubble, c is the speed of sound in the liquid, ρ_L is the density of the liquid, σ is the surface tension, μ is the liquid viscosity, p is the pressure inside the bubble, p_∞ is the ambient static pressure, P_A is the acoustic amplitude and f is the sound frequency. The acoustic amplitude P_A is correlated with the acoustic intensity I_a, or power per unit area, as $P_A = (2I_a\rho_L c)^{1/2}$ [28].

The expansion of the bubble is assumed as isothermal and its total compression is considered as adiabatic [29]. These assumptions, which are widely accepted since the lifetime of an oscillation at high frequency is relatively short with a very rapidly occurring collapse event, were pointed out by Yasui et al. [30] using a more detailed model. We also assume that the vapor pressure in the bubble remains constant during the bubble expansion phase and there is no gas diffusion during expansion and no mass and heat transfer of any kind during collapse. We note here that Storey and Szeri [31] demonstrated that the inclusion of mass transfer on the bubble dynamics has practically no effect on the maximum bubble temperature attained in the bubble at the collapse when the compression ratio of the bubble (R_{max}/R_{min}) is less than 20 (R_{max} is the maximum radius of the bubble and R_{min} is the minimum bubble radius at the collapse). This level of R_{max}/R_{min} was never attained in the present numerical study (see Table 4). Therefore, in order to reduce computational parameters, the current model takes, as input, initial bubble vapor content and neglects mass and heat transfer during bubble expansion and collapse.

Because of the above assumptions, the pressure and temperature inside the bubble at any instant during adiabatic phase can be calculated from the bubble size as

$$p=\left[P_v+P_{g0}\left(\frac{R_0}{R_{max}}\right)^3\right]\left(\frac{R_{max}}{R}\right)^{3\gamma} \quad (2)$$

$$T = T_\infty \left(\frac{R_{max}}{R}\right)^{3(\gamma-1)} \quad (3)$$

where P_v is the vapor pressure, $P_{g0} = p_\infty + (2\sigma/R_0) - P_v$ is the gas pressure in the bubble at its ambient state ($R = R_0$), R_0 is the ambient bubble radius, T_∞ is the bulk liquid temperature and γ is the ratio of specific heats capacities (c_p/c_v) of the gas/vapor mixture, given as

$$\gamma = \sum_{k=1}^{K} y_k \gamma_k \quad (4)$$

where y_k is the mole fraction of the species k at time corresponding to $R = R_{max}$ and γ_k is the ratio of specific heat capacities of the species k, which will be assumed constant. At the starting point of the adiabatic phase (at $R = R_{max}$), the bubble content is water vapor and dissolved gas (O_2, N_2 or air, which is a mixture of 20% O_2 and 80% N_2). At the last stage of the bubble collapse, the bubble temperature increases drastically to several thousand Kelvin, which induces chemical reactions and chemical products formation. In reality, the value of γ change instantaneously with the temperature (the c_p and c_v of each species in the bubble vary with the temperature) and the composition of the bubble during the bubble collapse. However, the variation of the bubble composition due to the chemical reaction is not important, particularly for frequencies above 355 kHz as can be seen in Fig. 3. For the other case (frequency below 355 kHz), the consumption of reactants is accompanied by the formation of the products (mainly ·OH, O and H_2) which have individual γ_k of the same order as those of reactants (Table 1). Therefore, we assumed that the diminution in γ from the consumption of reactants will be compensated from the formation of the products. Consequently, the variation of γ due to the variation of the bubble composition at the end of the collapse can be neglected. On the other hand, the variation of the bubble temperature from ambient temperature to several thousand Kelvin have not shown a significant decrease in the value of γ as can be concluded from Table 1 that shows the effect of the bubble temperature on the values of γ of the main species presented in the bubble at the collapse. Thus, the bubble temperature will not affect significantly the value of γ. As a conclusion, the expression of γ (Eq. (4)) included only the species trapped initially in the bubble (water vapor and dissolved gases).

It is important to notice also that the assumption of spatial uniform pressure and temperature inside the bubble is valid as long as inertia effects are negligible and the velocity of the bubble wall is below the speed of sound in the vapor/gas mixture. This assumption was justified in detail in the paper published by Kamath et al. [33]. In addition, Yasui et al. [30] and Fujikawa and Akamatzu [34] pointed out in their complete models which include heat transfer that the bubble temperature and pressure are roughly uniform except at a very thin layer, called thermal boundary, near the bubble wall. Also, using the Eqs. (2) and (3) indicate that the bubble collapsing process is thermodynamically reversible. This approximation can be justified by the fact that after each collapse, the bubble passes through an equilibrium state before a following expansion part.

Several physical properties (saturated vapor pressure, density, surface tension, viscosity and sound velocity) appear in the above equations. The equations for the physical properties of liquid water have been described in our previous work [24].

Table 1
Variation of the ratio of specific heat capacities γ for the species H_2O, O_2, N_2, H_2 and ·OH as function of temperature.*

Temperature (K)	293	500	1000	2000	4000
γ_{H_2O}	1.329	1.31	1.252	1.192	1.163
γ_{O_2}	1.396	1.366	1.313	1.282	1.25
γ_{N_2}	1.4	1.391	1.341	1.3	1.285
γ_{H_2}	1.4	1.396	1.381	1.321	1.27
γ_{OH}	1	1	1	1.04	1

* The calculations are based on: $\gamma_k = \frac{c_{p_k}}{c_{v_k}} = \frac{c_{p_k}/R}{c_{v_k}/R}$. Using $c_{pk} - c_{vk} = R$ for an ideal gas: $\gamma_k = \frac{c_{pk}/R}{c_{pk}/R-1}$. The c_{pk}/R of the kth species is given by the NASA-polynomial formula [32]: $c_{pk}/R = a_{1k} + a_{2k}T + a_{3k}T^2 + a_{4k}T^3 + a_{5k}T^4$. The constants $a_{1k},\ldots,a_{5k}$ are available in the Burcat's Thermodynamic Database [32] for a wide range of temperature (up to 5000 K).

2.2. Chemical kinetics model

In the present study, chemical reactions occurring inside O_2, H_2, air and N_2 bubbles are investigated. For O_2 and H_2 bubbles, a kinetic mechanism consisting in 25 chemical reactions and their backwards reactions (first 25 reactions of Table 2) [29,35] is taken into account involving O_2, H_2O, ·OH, H·, O, HO_2, O_3, H_2 and H_2O_2 species. For air and N_2 bubbles, a kinetic mechanism consisting in 73 chemical reactions and their backwards reactions (all reactions of Table 2) [35–37] is taken into account including, in addition to those involved in an O_2 bubble, N_2, N, NO, NO_2, NO_3, HNO_2, HNO_3, N_2O, HNO, NH, NH_2, NH_3, N_2H_2, N_2H_3, N_2H_4, N_2O_4 and N_2O_5 species. The scheme in Table 2 has been partially validated from hydrogen flame studies [38] as well as shock-tube and reactor-type experiments [39]. It has also been validated from studies of single bubble sonochemistry [40].

The chemical kinetics model consists of the reaction mechanism and determines the production of each species during the bubble collapse. Rate expressions for the chemical reactions consider elementary reversible reactions involving K chemical species, which can be represented in the general form as

$$\sum_{k=1}^{K} \upsilon'_{ki} X_k \leftrightarrow \sum_{k=1}^{K} \upsilon''_{ki} X_k \quad (5)$$

in which υ_{ki} in the stoichiometric coefficients of the ith reaction and X_k is the chemical symbol for the kth species. The superscript $'$ indicates forward stoichiometric coefficients, while $''$ indicates reverse stoichiometric coefficients. The production rate $\dot{w}_k$ of the kth species can be written as a summation of the rate of the variables for all reactions involving the kth species:

$$\dot{w}_k = \sum_{i=1}^{I} (\upsilon''_{ki} - \upsilon'_{ki}) r_i \qquad (k = 1, \ldots, K) \quad (6)$$

The rate r_i for the ith reaction is given by the difference of the forward and reverse rates as

$$r_i = k_{f_i} \prod_{k=1}^{K} [X_k]^{\upsilon'_{ki}} - k_{r_i} \prod_{k=1}^{K} [X_k]^{\upsilon''_{ki}} \quad (7)$$

where $[X_k]$ is the molar concentration of the kth species and k_{fi} and k_{ri} are the forward and reverse rate constants of the ith reaction, respectively. The forward and reverse rate constants for the ith reactions are assumed to have the following Arrhenius temperature dependence:

$$k_{f_i} = A_{f_i} T^{b_{f_i}} \exp\left(-\frac{E_{a_{fi}}}{R_g T}\right) \quad (8)$$

$$k_{r_i} = A_{r_i} T^{b_{ri}} \exp\left(-\frac{E_{a_{ri}}}{R_g T}\right) \quad (9)$$

where R_g is the universal gas constant, A_{fi} (A_{ri}) is the pre-exponential factor, b_{fi} (b_{ri}) is the temperature exponent and E_{fi} (E_{ri}) is the activation energy. Arrhenius parameters of each chemical reaction are presented in Table 2.

Table 2
Scheme of the possible chemical reactions inside a collapsing acoustic bubble [29,35–39]. *M* is the third body. Subscript "*f*" denotes the forward reaction and "*r*" denotes the reverse reaction. *A* is in ($cm^3\ mol^{-1}\ s^{-1}$) for two body reaction [($cm^6\ mol^{-2}\ s^{-1}$) for a three body reaction], and E_a is in ($cal\ mol^{-1}$). For some of the backward reactions, the constants are not listed. Those backward reactions are neglected in the present calculations.

N°	Reaction	A_f	b_f	E_{af}	A_r	b_r	E_{ar}
H/O reactions							
1	$H_2O + M \leftrightarrow H^{\cdot} + {}^{\cdot}OH + M$	1.912×10^{23}	−1.83	1.185×10^5	2.2×10^{22}	−2.0	0.0
2	$O_2 + M \leftrightarrow O + O + M$	4.515×10^{17}	−0.64	1.189×10^5	6.165×10^{15}	−0.5	0.0
3	${}^{\cdot}OH + M \leftrightarrow O + H^{\cdot} + M$	9.88×10^{17}	−0.74	1.021×10^5	4.714×10^{18}	−1.0	0.0
4	$H^{\cdot} + O_2 \leftrightarrow O + {}^{\cdot}OH$	1.915×10^{14}	0.0	1.644×10^4	5.481×10^{11}	0.39	-2.93×10^2
5	$H^{\cdot} + O_2 + M \leftrightarrow HO_2^{\cdot} + M$	1.475×10^{12}	0.6	0.0	3.09×10^{12}	0.53	4.887×10^4
6	$O + H_2O \leftrightarrow {}^{\cdot}OH + {}^{\cdot}OH$	2.97×10^6	2.02	1.34×10^4	1.465×10^5	2.11	-2.904×10^3
7	$HO_2^{\cdot} + H^{\cdot} \leftrightarrow H_2 + O_2$	1.66×10^{13}	0.0	8.23×10^2	3.164×10^{12}	0.35	5.551×10^4
8	$HO_2^{\cdot} + H^{\cdot} \leftrightarrow {}^{\cdot}OH + {}^{\cdot}OH$	7.079×10^{13}	0.0	2.95×10^2	2.027×10^{10}	0.72	3.684×10^4
9	$HO_2^{\cdot} + O \leftrightarrow {}^{\cdot}OH + O_2$	3.25×10^{13}	0.0	0.0	3.252×10^{12}	0.33	5.328×10^4
10	$HO_2^{\cdot} + {}^{\cdot}OH \leftrightarrow H_2O + O_2$	2.89×10^{13}	0.0	-4.97×10^2	5.861×10^{13}	0.24	6.908×10^4
11	$H_2 + M \leftrightarrow H^{\cdot} + H^{\cdot} + M$	4.577×10^{19}	−1.4	1.044×10^5	1.146×10^{20}	−1.68	8.2×10^2
12	$O + H_2 \leftrightarrow H^{\cdot} + {}^{\cdot}OH$	3.82×10^{12}	0.0	7.948×10^3	2.667×10^4	2.65	4.88×10^3
13	${}^{\cdot}OH + H_2 \leftrightarrow H^{\cdot} + H_2O$	2.16×10^8	1.52	3.45×10^3	2.298×10^9	1.40	1.832×10^4
14	$H_2O_2 + O_2 \leftrightarrow HO_2^{\cdot} + HO_2^{\cdot}$	4.634×10^{16}	−0.35	5.067×10^4	4.2×10^{14}	0.0	1.198×10^4
15	$H_2O_2 + M \leftrightarrow {}^{\cdot}OH + {}^{\cdot}OH + M$	2.951×10^{14}	0.0	4.843×10^4	1.0×10^{14}	−0.37	0.0
16	$H_2O_2 + H^{\cdot} \leftrightarrow H_2O + {}^{\cdot}OH$	2.410×10^{13}	0.0	3.97×10^3	1.269×10^8	1.31	7.141×10^4
17	$H_2O_2 + H^{\cdot} \leftrightarrow H_2 + HO_2^{\cdot}$	6.025×10^{13}	0.0	7.95×10^3	1.041×10^{11}	0.70	2.395×10^4
18	$H_2O_2 + O \leftrightarrow {}^{\cdot}OH + HO_2^{\cdot}$	9.550×10^6	2.0	3.97×10^3	8.66×10^3	2.68	1.856×10^4
19	$H_2O_2 + {}^{\cdot}OH \leftrightarrow H_2O + HO_2$	1.0×10^{12}	0.0	0.0	1.838×10^{10}	0.59	$3.089 \times \times 10^4$
20	$O_2 + O + M \leftrightarrow O_3 + M$	4.1×10^{12}	0.0	-2.114×10^3	2.48×10^{14}	0.0	2.286×10^4
21	$OH + O_2 + M \leftrightarrow + O_3 + H$	4.4×10^7	1.44	7.72×10^4	2.3×10^{11}	0.75	0.0
22	$O_3 + H \leftrightarrow HO_2 + O$	4.1×10^{12}	0.0	-2.114×10^3	–	–	–
23	$O_3 + O \leftrightarrow O_2 + O_2$	5.2×10^{12}	0.0	4.18×10^3	–	–	–
24	$O_3 + OH \leftrightarrow O_2 + HO_2$	7.8×10^7	0.0	1.92×10^3	–	–	–
25	$O_3 + HO_2 \leftrightarrow O_2 + O_2 + OH$	1.0×10^{11}	0.0	2.82×10^3	–	–	–
H/O/N reactions							
26	$N_2 + M \leftrightarrow N + N + M$	3.7×10^{21}	−1.6	2.264×10^5	3.0×10^{14}	0.0	-1.0×10^3
27	$N_2 + O_2 \leftrightarrow N_2O + O$	6.3×10^{13}	0.0	1.104×10^5	1.0×10^{14}	0.0	2.82×10^4
28	$N_2O + H \leftrightarrow + N_2 + OH$	6.7×10^{13}	0.0	1.52×10^4	2.5×10^{12}	0.0	7.8×10^4
29	$NO_2 + M \leftrightarrow O + NO + M$	1.1×10^{16}	0.0	6.6×10^4	1.1×10^{15}	0.0	-1.88×10^3
30	$O_2 + N \leftrightarrow O + NO$	6.4×10^9	1.0	6.3×10^3	1.5×10^9	1.0	3.9×10^4
31	$NO_2 + H \leftrightarrow OH + NO$	3.5×10^{14}	0.0	1.48×10^3	2.0×10^{11}	0.5	3.1×10^4
32	$NO + HO_2 \leftrightarrow OH + NO_2$	3.0×10^{12}	0.5	2.4×10^3	1.0×10^{11}	0.5	1.2×10^4
33	$N_2O + O \leftrightarrow NO + NO$	1.0×10^{14}	0.0	2.82×10^4	1.30×10^{12}	0.0	6.420×10^4
34	$N_2O + M \leftrightarrow N_2 + O + M$	5.0×10^{14}	0.0	5.8×10^4	1.40×10^{12}	0.0	2.08×10^4
35	$O + N_2 \leftrightarrow NO + N$	7.60×10^{13}	0.0	7.60×10^4	1.60×10^{13}	0.0	0.00
36	$O + NO_2 \leftrightarrow O_2 + NO$	1.0×10^{13}	0.0	6.0×10^2	1.70×10^{12}	0.0	4.680×10^4
37	$N + OH \leftrightarrow H + NO$	4.5×10^{13}	0.0	0.00	1.70×10^{14}	0.0	4.90×10^4
38	$N + O_3 \leftrightarrow NO + O_2$	1.2×10^{12}	0.5	2.40×10^3	–	–	–
39	$NO + NO_3 \leftrightarrow NO_2 + NO_2$	4.1×10^{14}	0.0	9.62×10^2	3.90×10^{11}	0.0	2.400×10^4
40	$NO + M \leftrightarrow N + O + M$	4.0×10^{20}	−1.5	1.51×10^5	6.40×10^{16}	−0.5	0.00
41	$OH + NO + M \leftrightarrow HNO_2 + M$	8.0×10^{15}	0.0	-1.0×10^3	5.10×10^{17}	−1.0	5.000×10^4
42	$OH + HNO_2 \leftrightarrow H_2O + NO_2$	1.5×10^{12}	0.0	5.60×10^1	8.40×10^{11}	0.0	4.227×10^4
43	$HNO_2 + O \leftrightarrow OH + NO_2$	6.0×10^{11}	0.0	4.0×10^3	–	–	–
44	$HNO_2 + H \leftrightarrow H_2 + NO_2$	4.9×10^{11}	0.5	3.00×10^3	2.40×10^{13}	0.0	2.90×10^4
45	$O + HNO_2 \leftrightarrow HNO + O_2$	3.0×10^{12}	0.0	1.60×10^4	–	–	–
46	$OH + NO_2 + M \leftrightarrow HNO_3 + M$	5.0×10^{17}	0.0	0.0	1.6×10^{15}	0.0	3.08×10^4
47	$HNO_3 + O \leftrightarrow OH + NO_3$	6.0×10^{11}	0.0	8.0×10^3	–	–	–
48	$O + HNO_3 \leftrightarrow O_2 + HNO_2$	6.0×10^{12}	0.0	1.6×10^4	–	–	–
49	$HNO + M \leftrightarrow H + NO + M$	3.0×10^{16}	0.0	4.9×10^4	5.4×10^{15}	0.0	-3.0×10^2
50	$NO_2 + O + M \leftrightarrow NO_3 + M$	1.1×10^{19}	0.0	0.0	2.5×10^9	0.0	0.0
51	$NO_3 + H \leftrightarrow OH + NO_2$	3.5×10^{14}	0.0	1.5×10^3	–	–	–
52	$HNO + O \leftrightarrow OH + NO$	4.9×10^{11}	0.5	2.0×10^3	–	–	–
53	$NO_2 + N \leftrightarrow NO + NO$	6.3×10^{14}	0.0	0.0	9.0×10^9	0.5	7.839×10^4
54	$NO_2 + N \leftrightarrow N_2O + O$	4.7×10^{12}	0.0	0.0	–	–	–
55	$NO_2 + N \leftrightarrow N_2 + O_2$	1.1×10^{12}	0.0	0.0	–	–	–
56	$NO_2 + N \leftrightarrow N_2 + 2O$	1.4×10^{12}	0.0	0.0	–	–	–
57	$NO + NO + O_2 \leftrightarrow NO_2 + NO_2$	1.2×10^9	0.0	-1.06×10^3	2.00×10^{12}	0.0	2.70×10^4
58	$NO_3 + NO_3 \leftrightarrow 2NO_2 + O_2$	6.1×10^{12}	0.0	6.0×10^3	–	–	–
59	$HNO + H \leftrightarrow H_2 + NO$	4.8×10^{12}	0.0	0.0	1.4×10^{13}	0.0	5.526×10^4
60	$HNO + OH \leftrightarrow NO + H_2O$	6.3×10^{13}	0.0	0.0	2.40×10^6	0.0	5.0×10^3
61	$HNO_3 + OH \leftrightarrow H_2O + NO_3$	8.0×10^{10}	0.0	0.0	1.40×10^{-2}	0.0	-2.237×10^4
62	$NH_3 + M \leftrightarrow H + NH_2$	9.2×10^{15}	0.0	8.48×10^4	–	–	–
63	$NH_3 + H \leftrightarrow H_2 + NH_2$	1.0×10^{12}	0.0	6.28×10^3	–	–	–
64	$NH_3 + O \leftrightarrow NH_2 + OH$	1.5×10^{12}	0.0	6.04×10^3	–	–	–
65	$NH_3 + OH \leftrightarrow H_2O + NH_2$	2.0×10^{13}	0.0	3.006×10^3	–	–	–
66	$NH_2 + OH \leftrightarrow H_2O + NH$	3.0×10^{10}	0.679	1.3×10^3	–	–	–
67	$NH_2 + NH_2 \leftrightarrow NH_3 + NH$	4.0×10^{10}	0.0	5.60×10^3	–	–	–
68	$N_2H_4 + H \leftrightarrow H_2 + N_2H_3$	1.3×10^{13}	0.0	5.520	–	–	–
69	$N_2H_4 + M \leftrightarrow NH_2 + NH_2 + M$	4.0×10^{15}	0.0	4.12×10^4	1.0×10^{16}	0.0	0.0
70	$N_2H_4 + O \leftrightarrow H_2O + N_2H_2$	7.1×10^{13}	0.0	1.20×10^3	–	–	–

Table 2 (*continued*)

N°	Reaction	A_f	b_f	E_{af}	A_r	b_r	E_{ar}
71	$N_2H_4 + NH_2 \leftrightarrow NH_3 + N_2H_3$	1.0×10^{13}	0.0	5.6×10^3	3.3×10^6	0.0	0.0
72	$N_2O_4 + M \leftrightarrow NO_2 + NO_2 + M$	1.8×10^{17}	0.0	1.11×10^4	1.7×10^{13}	0.0	1.72×10^3
73	$N_2O_5 + M \leftrightarrow NO_2 + NO_3 + M$	1.3×10^{19}	0.0	1.944×10^4	2.0×10^{17}	0.0	-9.62×10^2

Table 3
Selected values of the ambient radius (R_0) for active bubbles as function of frequency of ultrasound, selected according to experimental data.

Frequency (kHz)	Ambient bubble radius, R_0 (μm)	Refs.
213	3.9	[18]
355	3.2	[18]
515	3	[44]
647	2.9	[18]
875	2.7	[18]
1000	2	[18]
1100	1.4	[45]

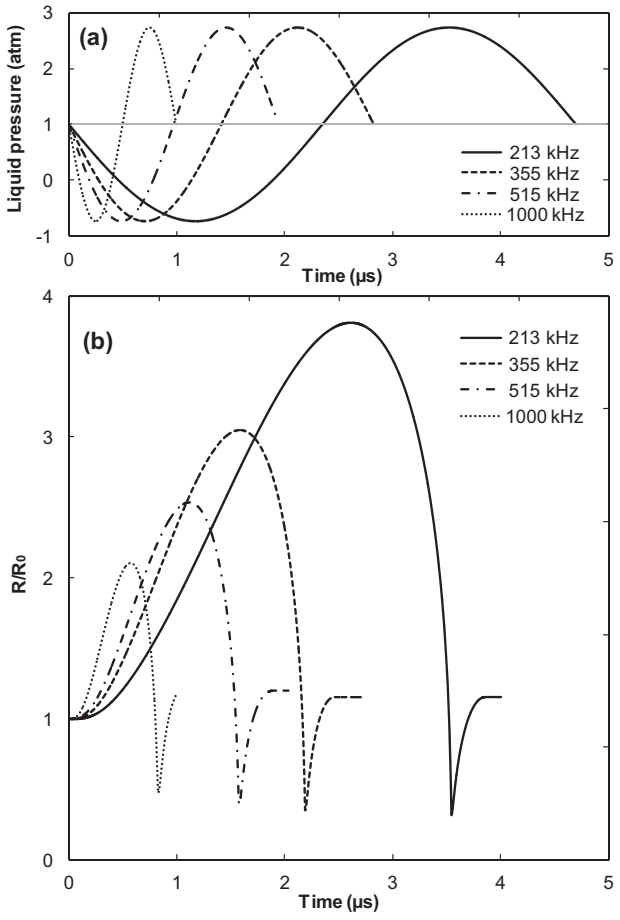

Fig. 1. Liquid pressure (a) and R/R_0 (b) versus time curves for one acoustic cycle at various ultrasonic frequencies (conditions: ambient bubble radius: Table 3; acoustic intensity: 1 W cm^{-2}; bulk liquid temperature: 20 °C; static pressure: 1 atm). The liquid pressure in (a) is the sum of the acoustic pressure $-P_A \sin 2\pi ft$ and the static pressure P_∞.

2.3. Procedure of the numerical simulation

The simulation of the reactions system (Table 2) occurring in the bubble starts at the beginning of the adiabatic phase (time corresponding to R_{max}). The input parameters of the reactions system are the composition of the bubble on water vapor and gas at this point, the temperature and pressure profiles in the bubble during adiabatic phase and the collapse time. All these parameters were obtained by solving the dynamics equation (Eq. (1)). The bubble temperature increases during the adiabatic phase, the reaction system evolves and radicals start to form by thermal dissociation of H_2O and gas molecules in the bubble. Thus, the composition of the bubble for all species expected to be present was determined at any temperature during the collapse phase. The simulation of the reactions system was stopped after the end of the bubble collapse. It should be also noticed that the effect of the chemical reaction (heat of reaction) occurring in the cavity on the bubble dynamics is known to be not significant [31,41]. The dynamics output results, thus, will not greatly affected by the chemical reactions. This effect is not taken into account in the present numerical investigation.

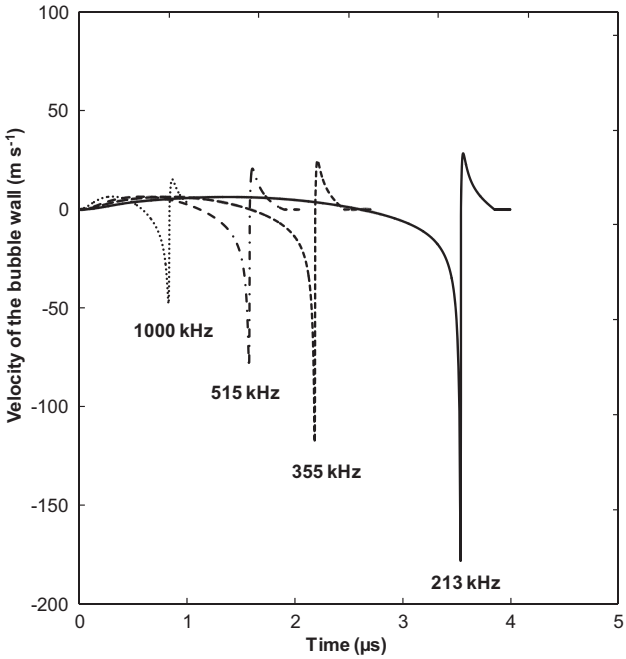

Fig. 2. Bubble wall velocity as function of time during the oscillation of the bubble for different ultrasonic frequencies, for the same conditions as in Fig. 1.

3. Results and discussion

According to the experimental and theoretical data [18,19,42,43], it is now well known that the ambient radius (R_0) for a typical active bubble depends on the experimentally controllable parameters such as the driving ultrasonic frequency. The range of ambient bubble radius for a typical active bubble is rather narrow according to the experimental observations and in this range there exists an ambient radius at which the most activity is localized [18]. The ambient bubble radius at which the activity is localized is called mean ambient bubble radius. The mean ambient bubble radius decreases considerably as the ultrasonic frequency increases in the range 213–1100 kHz according to the experimental observations [18]. The present study tries to use the same frequencies at which the mean ambient bubble radii (R_0) were determined

experimentally. The ambient bubble radius (R_0) in the present numerical simulations has been assumed as the mean ambient bubble radius. The selected values of R_0 with respect to the ultrasonic frequency are presented in Table 3.

3.1. Bubble dynamics and chemical bubble yield

In Fig. 1(a) and (b), the calculated results of the liquid pressure and the R/R_0 ratio for one acoustic cycle are shown for ultrasonic frequencies of 213, 355, 515 and 1000 kHz when the acoustic intensity is 1 W cm^{-2}. The time axes in Fig. 1(a) and (b) are identical. The liquid pressure applied on the bubble is the sum of the acoustic pressure and the static pressure. In all cases, the bubble starts from an ambient radius of R_0 which is the radius at which the bubble is in static mechanical equilibrium with the external static pressure (typically 1 atm). It was seen that the bubble initially expands during the rarefaction phase of ultrasound wave, reaches a maximum at the beginning of the compression phase and then quickly collapses during the compression phase of ultrasound wave. The minimum bubble radius, which indicates the end of the bubble collapse, is attained when the liquid pressure is at around of its maximum value (2.72 atm) during the compression phase. Fig. 1 clearly shows that the bubble dynamics is strongly affected by the ultrasonic frequency. From the first view, it was noticed that the maximum bubble radius and the bubble lifetime decrease as the frequency increases.

The velocity of the bubble wall during oscillation, especially at the collapse, is a very important parameter that gives an idea about the quality of implosion. Fig. 2 shows the behavior of the bubble wall speed as function of time for the same conditions as in Fig. 1. Insignificant changes of the bubble wall velocity are observed during the expansion phase and the first stage of the collapse. However, the bubble wall velocity increases suddenly during the final stage of the bubble collapse up to 178, 118, 78 and 48 m s^{-1} for respectively 213, 355, 515 and 1000 kHz. These high speeds of the bubble implosion yield stronger collapses, which

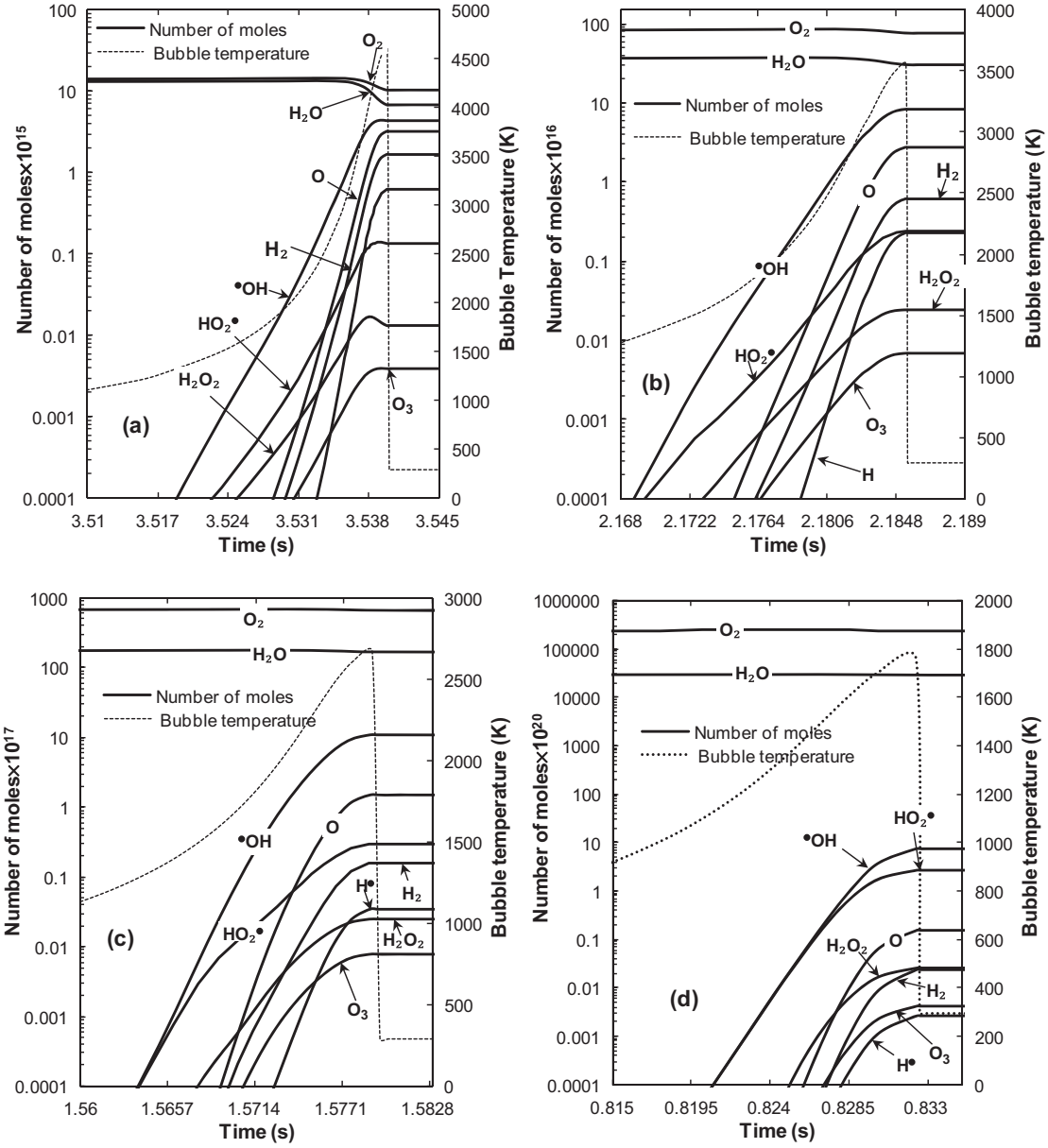

Fig. 3. Evolution of the reaction systems inside a bubble as function of time at around the end of the bubble collapse for various ultrasonic frequencies, for the same conditions as in Fig. 1. (a) 213 kHz, (b) 355 kHz, (c) 515 kHz and (d) 1000 kHz. Horizontal axes are presented for only ~0.015 μs. Principal vertical axes are in logarithmic scale. The dominant oxidant created in all cases is ·OH radical.

generate extremely higher conditions inside the bubbles. Indeed, the bubble internal pressure may increase up to 1237, 578, 280 and 106 atm at the end of the bubble collapse for respectively 213, 355, 515 and 1000 kHz.

In Fig. 3(a)–(d), the calculated results of the bubble core temperature and the chemical reactions inside a bubble are shown as function of time at around the end of the bubble collapse for the studied ultrasonic frequencies. It is seen that the bubble core is heated up to 4615, 3557, 2672 and 1785 K at the end of the bubble collapse for 213, 355, 515 and 1000 kHz, respectively. These conditions promote chemical reactions in the bubble as illustrated in Fig. 3(a)–(d). Large amounts of the trapped water vapor and oxygen are dissociated and many chemical oxidants such as ·OH, O, H·, HO_2·, H_2O_2 and O_3 are created in the bubble. It is seen that hydroxyl radical (·OH) is the main oxidant created in the bubble. HO_2, H_2O_2 and O_3 are not formed at appreciable amounts in the bubble. It is also seen from Fig. 3(a)–(d) that the higher the maximum bubble temperature (T_{max}) attained at the end of the bubble collapse, the higher will be the amount of each oxidants created in the bubble. The amount of each chemical oxidant attained an upper limit at the end of the bubble collapse, followed by almost constant production after the end of the bubble collapse as the bubble temperature decreases suddenly. Another important statement to be noted from Fig. 3(a)–(d) is that all the chemical reactions inside a bubble occur in time scale of about 0.015 μs (15 ns), which represents only about 1–5% of the collapse time of the bubble (τ_c).

3.2. Effect of ultrasonic frequency on the chemical bubble yield

The effect of ultrasonic frequency (213–1100 kHz) on the production rate of each oxidant created inside a collapsing O_2-bubble is shown in Fig. 4 for an acoustic intensity of 1 W cm^{-2} and bulk liquid temperature of 20 °C. The vertical axis in this figure is in logarithmic scale. In Figs. 4 and 5, the production rate of each

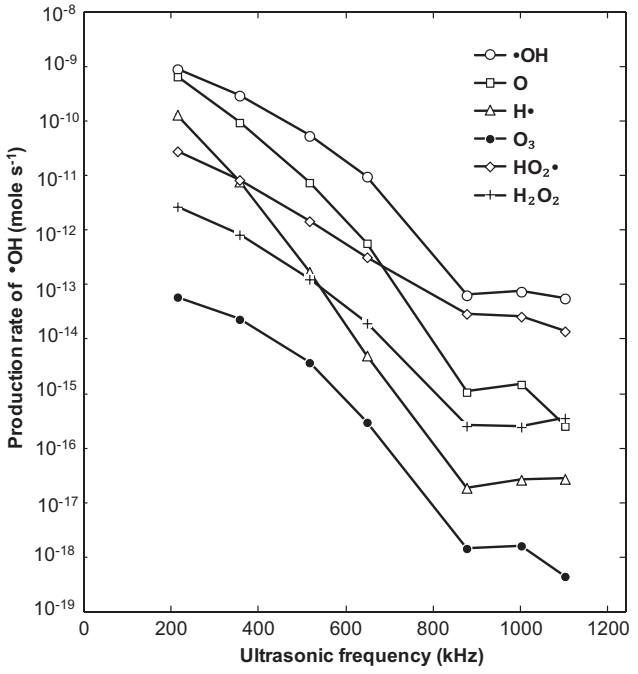

Fig. 4. Production rate of each chemical oxidant created inside a collapsing O_2-bubble as function of ultrasonic frequency (conditions: ambient bubble radius: Table 3; acoustic intensity: 1 W cm^{-2}; bulk liquid temperature: 20 °C; static pressure: 1 atm). The vertical axis is in logarithmic scale. The production rate for each oxidant is defined as the amount of this species at the end of the first bubble collapse multiplied by the ultrasonic frequency [43].

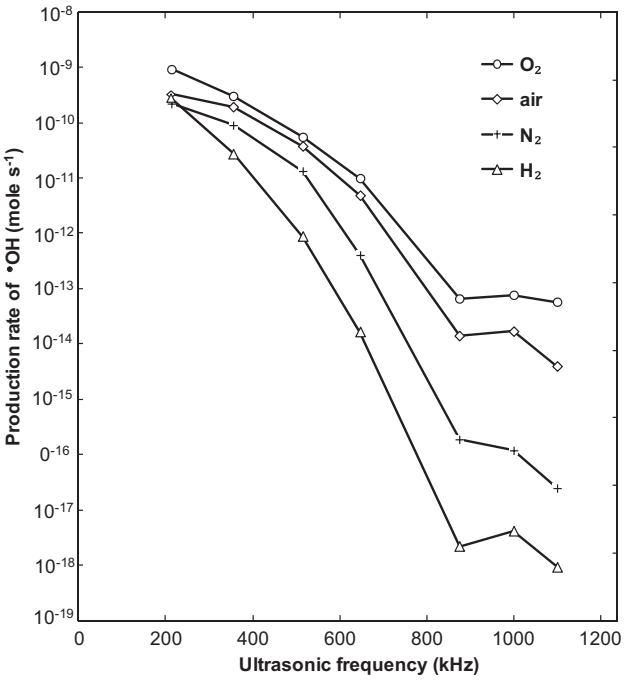

Fig. 5. Production rate of ·OH radical inside a bubble as function of ultrasonic frequency for various saturating gases (conditions: ambient bubble radius: Table 3; acoustic intensity:1 W cm^{-2}; bulk liquid temperature: 20 °C; static pressure: 1 atm). The vertical axis is in logarithmic scale. The production rate of ·OH is defined as the amount of this species at the end of the first bubble collapse multiplied by the ultrasonic frequency [43].

chemical oxidant is the amount of the species inside a bubble at the end of the first bubble collapse multiplied by ultrasonic frequency [43]. According to Fig. 4, the general trend is that the production rate of each oxidant created in the bubble is higher at lower ultrasonic frequency. This result may be a consequence of a number of factors that are sensitively affected by the variation of ultrasound frequency. This includes the maximum bubble core temperature (T_{max}) and pressure (p_{max}) achieved in the bubble at the end of the collapse, the amount of water vapor trapped at the collapse and the expansion and collapse times of the bubble. Table 4 illustrates how ultrasonic frequency affects these dynamics parameters. Because a smaller frequency gives the bubble more time to expand, it leads to a larger expansion ratio (R_{max}/R_0) and so higher compression ratio (R_{max}/R_{min}) as can be seen in Table 4. As a result, the collapse will be stronger and generates higher T_{max} and p_{max} (Table 4) and this accelerates the dissociation of water vapor and oxygen molecules into free radicals and atoms. However, simultaneously, the expansion to a larger expansion radius is accompanied by a larger amount of vapor being trapped during collapse (Table 4), which decreases γ of the mixture and thus decreases T_{max} and p_{max}. However, for high frequencies (above 100 kHz), the first mechanism dominates, and the net effect of decreasing frequency is an increase in T_{max} and p_{max} as shown in Table 4. Another important factor responsible for the trend observed in Fig. 4 is the shorter collapse time (τ_c) at higher frequencies (see Table 4). In this situation, the reactions system inside a bubble has not enough time to evolve and then convert reactant molecules to free radical and atoms.

Therefore, the decrease of the maximum bubble core temperature (T_{max}) and pressure (p_{max}) and the collapse time of the bubble (τ_c) with increasing frequency would thus result in lower dissociation of H_2O and O_2 molecules and this lowers the production rate of the chemical oxidants inside a bubble as indicated in Fig. 3. We would like to mention here that the frequency of 875 kHz seems to be abnormal as the tendency changes at this frequency

Table 4
Evolutions of the bubble dynamics parameters as function of ultrasonic frequency. (τ_{exp}) is the expansion time of the bubble, (R_{max}/R_0) is the expansion ratio of the bubble, (R_{max}/R_{min}) is the compression ratio of the bubble, T_{max} and p_{max} are, respectively, the maximum bubble temperature and pressure reached in the bubble at the end of the collapse, y_{H_2O} is the mole fraction of water vapor trapped at the collapse and (τ_c) is the collapse time of the bubble.

Frequency	τ_{exp} (μs)	R_{max}/R_0	R_{max}/R_{min}	T_{max} (K)	P_{max} (atm)	y_{H_2O}	τ_c (μs)
213	2.609	3.808	11.871	4615.96	1237.41	0.482	0.930
355	1.583	3.049	8.677	3557.72	578.03	0.310	0.603
515	1.117	2.532	6.494	2672.59	280.18	0.202	0.462
647	0.907	2.272	5.397	2190.47	173.92	0.153	0.398
875	0.687	2.008	4.281	1687.38	94.29	0.108	0.328
1000	0.575	2.107	4.434	1758.88	106.61	0.111	0.25
1100	0.486	2.231	4.384	1734.7	101.08	0.111	0.201

(Figs. 4 and 5). This result is theoretically logical as the maximum bubble temperature present a minimum at this point as shown in Table 4. Practically, we attribute this phenomenon to an error in the experimental value of R_0 at 875 kHz (2.7 μm). According to the procedure presented in Ref. [19], the value of R_0 at 875 kHz should be near 2 μm, which yield a maximum bubble temperature of 1970 K. This temperature is lower than that of 647 kHz (2190 K) and higher than that of 1000 kHz (1758 K), which will yield a normal tendency in Figs. 4 and 5. In the numerical simulations, we retained the experimental value of 2.7 μm.

After knowing the effects of frequency on single bubble yield, we will discuss briefly its effects on the sonochemical activity in aqueous solution. Some experimental reports [8,9,15,16,46] showed the existence of an optimum frequency between 200 and 1000 kHz that maximize the overall sonochemical activity. A this level, we say that aqueous solution is a multibubble system and the overall sonochemical activity in multibubble system is not related only to the single bubble event, but also to the number of bubbles and other phenomena (i.e., bubbles coalescence). The number of bubbles formed in the cavitating medium is strongly affected by the applied ultrasonic frequency. Generally, the number of bubbles increases as the applied frequency increases [11,21]. Therefore, the chance of existing of an optimum frequency between 200 and 1000 kHz for the production of the oxidants in aqueous solution is possible as the sonochemical activity in individual bubble decreases with increasing frequency in this interval whereas the number of bubbles increases with increasing frequency. However, in the absence of exact information about the bubble population, any theoretical decision about the existing of an optimum frequency is not possible to make.

3.3. Effect of the nature of dissolved gas on the chemical bubble yield

Numerical simulations of chemical reactions occurring in the bubble during implosion have been performed for different saturating gases including O_2, air, N_2 and H_2. In all cases, the numerical calculations showed that ·OH radical is the main powerful oxidant created in the bubble. The production rate of hydroxyl radical (·OH) will thus used in the following for comparison.

In Fig. 5, the effects of the selected dissolved gases (O_2, air, N_2 and H_2) on the production rate of ·OH radical in the bubble are shown for various ultrasonic frequencies. The same general trend of decreasing production rate of ·OH radical with increasing frequency is observed for all the saturating gases. From Fig. 5, it is clearly appeared that the effect of saturating gases on the production rate of ·OH radical follows the order O_2 > air > N_2 > H_2. The other trend to be noted from Fig. 5 is that the effect of saturating gases on the production rate of ·OH radical becomes more remarkable at higher ultrasonic frequencies.

In the literature, several experimental reports [12,13,17,47,48] conducted at different frequencies in the range of 300–1000 kHz showed that the sonochemical production of H_2O_2 and the degradation of various non-volatile organic contaminants in aqueous solutions followed the order O_2 > air > N_2 > H_2. Therefore, the obtained results in this study for single bubble sonochemistry that is consistent qualitatively with the experimental results, should explain with arguments the effects of saturating gases on the sonochemical activity.

In general, dissolved gases affect the single bubble sonochemistry through two aspect: (i) gas with higher polytropic ratio γ ($\gamma = c_p/c_v$) can create higher maximum temperature (T_{max}) at the collapse, which enhances the dissociation of water vapor molecules trapped in the bubble at the collapse; (ii) gases with low thermal conductivities (λ) can reduce the heat dissipation, thus facilitating the increase in collapse temperature (T_{max}) and enhancing sonochemical activity. In this study, all employed gases have the same polytropic ratio ($\gamma = 1.41$) and O_2, N_2 and air have the same thermal conductivity ($\lambda = 0.026$ W m^{-2} K^{-1} [49]). Therefore, the intensity of the bubble implosion will be identical for all the employed gases and the maximum bubble temperature (T_{max}) achieved at the collapse is the same. The values of T_{max} with respect to frequency are the same as those of Table 4. It should also be noted here that Okitsu et al. [20] showed experimentally that the bubble temperature is not affected by the gas conductivity. Excluding the effects of gases on the maximum bubble temperature (T_{max}) achieved at the collapse, the observed effects of saturating gases on single bubble sonochemistry (Fig. 5) are thus associated only to the nature of the reactants trapped in the bubble at the collapse (O_2/H_2O, $O_2/N_2/H_2O$, N_2/H_2O, H_2/H_2O) which affects directly the internal bubble-chemistry. Using the chemical kinetics analysis, some explanation can be made. In the case of O_2 and H_2 bubbles, ·OH radical was consumed mainly though the following reactions: $\cdot OH + H\cdot \leftrightarrow O + H_2$ and $\cdot OH + H_2 \leftrightarrow H + H_2O$. In the case of air and N_2 bubbles, an additional reaction involved NO species contributed significantly in the consumption of ·OH radical. This reaction is $NO + \cdot OH + M \leftrightarrow HNO_2 + M$. On the other hand, NO was formed mainly through $NO_2 + M \leftrightarrow O + NO + M$ and $N_2 + O \leftrightarrow NO + N$. Consequently, the higher the concentration of N_2 in the bubble, the higher will be the concentration of NO and this accelerates the consumption rate of ·OH radical thought the reaction $NO + \cdot OH + M \leftrightarrow HNO_2 + M$. Therefore, it is not surprising that between O_2, air and N_2, the production rate of ·OH radical follows the order O_2 > air > N_2 as the concentration of N_2 decreases in the same order. The inhibiting effect of oxidizing nitrogen (NO) toward the production of the oxidants inside an air bubble have been previously reported by Yasui et al. [50]. Between H_2 and other gases, the problem is treated in similar manner. The higher the concentration of H_2 in the bubble, the higher will be the scavenging rate of ·OH radical thought the reaction $\cdot OH + H_2 \leftrightarrow H\cdot + H_2O$. Thus, it is very logical that hydrogen occupied the last class in the order O_2 > air > N_2 > H_2 as the concentration of hydrogen is the highest in the case of hydrogen bubble.

Knowledge the order of saturating gases on single bubble sonochemistry allows the discussion of their effects in aqueous

solutions (multibubble systems). In this case, the solubility of the gas is an important factor because it control the number of collapsing bubbles and the higher the gas solubility, the higher will be the number of bubbles formed in the reactor. The solubilities (in mole fraction) of the gases treated in the present numerical study are [51]: $x_{O_2} = 2.517 \times 10^{-5}$, $x_{air} = 1.524 \times 10^{-5}$, $x_{N_2} = 1.276 \times 10^{-5}$, $x_{H_2} = 1.457 \times 10^{-5}$. Therefore, the order of the solubility follows $O_2 > air > H_2 > N_2$. This order constitutes a fort indication that the overall sonochemical activity in aqueous solutions is not controlled by the gas solubility alone, as pointed by Okutso et al. [20], but also by the nature of the internal bubble chemistry because H_2 have a high solubility than N_2 but it yielded the lower overall sonochemical activity (see Ref. [48]). This is in a fact because H_2 yielded the lowest activity in the scale of single bubble (Fig. 5). Consequently, in addition to the gas solubility, the nature of the internal bubble chemistry is another parameter of a paramount importance that controls the overall sonochemical activity of ultrasound in aqueous solutions.

4. Conclusion

In this work, results from a comprehensive numerical assessment of frequency and gas effects on sonochemical activity of single bubble have been described. The numerical simulations of the bubble oscillations and chemical reactions therein have been performed for various ultrasonic frequencies (in the range of 213–1100 kHz) under different saturating gases (O_2, air, N_2 and H_2). The results of this study provide a detailed informations about the gas and frequency mechanisms on single bubble sonochemistry, which will help in understanding their effects in aqueous solutions. The effect of ultrasonic frequency on single bubble sonochemistry was attributed to its significant impact on the cavitation process whereas the effect of gases was attributed to the nature of the combustion chemistry occurred in the bubble (Ar/H_2O, O_2/H_2O, H_2/H_2O...). It is concluded that the nature of the bubble chemistry is an additional parameter that controls the overall sonochemical activity of ultrasound in aqueous solutions. The understanding of the frequency effect on sonochemical activity in aqueous solutions needs the knowledge of the number of bubbles created in the liquid. However, in absence of sufficiently information about the number of bubbles created in the sonicating medium, any theoretical decision about the effect of frequency on the overall sonochemical activity of ultrasound in aqueous solutions is not possible to make.

Acknowledgments

The financial support by the Ministry of Higher Education and Scientific Research of Algeria (Project No. J0101120120098) is greatly acknowledged.

References

[1] K.S. Suslick, Y. Didenko, M.M. Fang, T. Hyeon, K.J. Kolbeck, W.B. McNamara, M.M. Mdleleni, M.M. Wong, Acoustic cavitation and its chemical consequences, Philos. Trans. R. Soc. A: Math. Phys. Eng. Sci. 357 (1999) 335–353.
[2] K.S. Suslick, D.A. Hammerton, R.E.J. Cline, Sonochemical hotspot, J. Am. Chem. Soc. 108 (1986) 5641–5642.
[3] K.S. Suslick, D.J. Flannigan, Inside a collapsing bubble: sonoluminescence and the conditions during cavitation, Annu. Rev. Phys. Chem. 59 (2008) 659–683.
[4] T. Leong, M. Ashokkumar, S. Kentish, The fundamentals of power ultrasound–a review, Acoust. Aust. 39 (2011) 54–63.
[5] Y.G. Adewuyi, Sonochemistry: environmental science and engineering applications, Ind. Eng. Chem. Res. 40 (2001) 4681–4715.
[6] S.J. Putterman, K.R. Weninger, Sonoluminescence: how bubbles turn sound into light, Annu. Rev. Fluid Mech. 32 (2000) 445–476.
[7] F.R. Young, Sonoluminescence, CRC Press, Boca Raton, Florida, 2005.
[8] M. Capocelli, E. Joyce, A. Lancia, T.J. Mason, D. Musmarra, M. Prisciandaro, Sonochemical degradation of estradiols: incidence of ultrasonic frequency, Chem. Eng. J. 210 (2012) 9–17.
[9] M. Dukkanci, M. Vinatoru, T.J. Maison, Sonochemical treatment of orange II using ultrasound at range of frequencies and powers, J. Adv. Oxid. Technol. 15 (2012) 277–283.
[10] T.J. Mason, A.J. Cobley, J.E. Graves, D. Morgan, New evidence for the inverse dependence of mechanical and chemical effects on the frequency of ultrasound, Ultrason. Sonochem. 18 (2011) 226–230.
[11] P. Kanthale, F. Ashokkumar, F. Grieser, Sonoluminescence, sonochemistry (H_2O_2 yield) and bubble dynamics: frequency and power effects, Ultrason. Sonochem. 15 (2008) 143–150.
[12] F. Méndez-Arriaga, R.A. Torres, C. Pétrier, S. Esplugas, J. Gimenez, C. Pulgarin, Ultrasonic treatment of water contaminated with ibuprofen, Water Res. 42 (2008) 4243–4248.
[13] R.A. Torres, C. Pétrier, E. Combet, M. Carrier, C. Pulgarin, Ultrasonic cavitation applied to the treatment of bisphenol A. Effect of sonochemical parameters and analysis of BPA by-products, Ultrason. Sonochem. 15 (2008) 605–611.
[14] Y. Jiang, C. Petrier, T.D. Waite, Sonolysis of 4-chlorophenol in aqueous solution: effects of substrate concentration, aqueous temperature and ultrasonic frequency, Ultrason. Sonochem. 13 (2006) 415–422.
[15] S. Koda, T. Kimura, T. Kondo, H. Mitome, A standard method to calibrate sonochemical efficiency of an individual reaction system, Ultrason. Sonochem. 10 (2003) 149–156.
[16] M.A. Beckett, I. Hua, Impact of ultrasonic frequency on aqueous sonoluminescence and sonochemistry, J. Phys. Chem. A 105 (2001) 3796–3802.
[17] E.L. Mead, R.G. Sutherland, R.E. Verrall, The effects of ultrasound on water in the presence of dissolved gases, Can. J. Chem. 54 (1976) 1114–1120.
[18] A. Brotchie, F. Grieser, M. Ashokkumar, Effect of power and frequency on bubble-size distributions in acoustic cavitation, Phys. Rev. Lett. 102 (2009) 084302-1–084302-4.
[19] S. Merouani, O. Hamdaoui, Y. Rezgui, M. Guemini, Effects of ultrasound frequency and acoustic amplitude on the size of sonochemically active bubbles-theoretical study, Ultrason. Sonochem. 20 (2013) 815–819.
[20] K. Okitsu, T. Suzuki, N. Takenaka, H. Bandow, R. Nishimura, Y. Maeda, Acoustic multibubble cavitation in water: a new aspect of the effect of a rare gas atmosphere on bubble temperature and its relevance to sonochemistry, J. Phys. Chem. B 110 (2006) 20081–20084.
[22] S. Merouani, O. Hamdaoui, Y. Rezgui, M. Guemini, Theoretical estimation of the temperature and pressure within collapsing acoustical bubbles, Ultrason. Sonochem. 21 (2014) 53–59.
[23] S. Merouani, O. Hamdaoui, Y. Rezgui, M. Guemini, Energy analysis during acoustic bubble oscillations: relationship between bubble energy and sonochemical parameters, Ultrasonics 54 (2014) 227–232.
[24] S. Merouani, O. Hamdaoui, Y. Rezgui, M. Guemini, Computer simulation of chemical reactions occurring in collapsing acoustical bubble: dependence of free radicals production on operational conditions, Res. Chem. Intermed. (2013), http://dx.doi.org/10.1007/s11164-013-1240-y.
[25] L.A. Crum, The polytrophic exponent of gas contained within air bubbles pulsating in a liquid, J. Acoust. Soc. Am. 73 (1983) 116–120.
[26] J.B. Keller, I.I. Kolodner, Damping of underwater explosion bubble oscillations, J. Appl. Phys. 27 (1956) 1152–1161.
[27] J.B. Keller, M.J. Miksis, Bubble oscillations of large amplitude, J. Acoust. Soc. Am. 68 (1980) 628–633.
[28] T.G. Leighton, The Acoustic Bubble, Academic Press, London, UK, 1994.
[29] A.J. Colussi, L.K. Weavers, M.R. Hoffmann, Chemical bubble dynamics and quantitative sonochemistry, J. Phys. Chem. A 102 (1998) 6927–6934.
[30] K. Yasui, Effect of non-equilibrium evaporation and condensation on bubble dynamics near the sonoluminescence threshold, Ultrasonics 36 (1998) 575–580.
[31] B.D. Storey, A.J. Szeri, Water vapor, sonoluminescence and sonochemistry, Proc. R. Soc. London, Sect. A 456 (2000) 1685–1709.
[32] Burcat's Thermodynamical Database, ftp://ftp.technion.ac.il/pub/supported/aetdd/thermodyna- mics/; also available from; http://garfield.chem.elte.hu/Burcat/burcat.html.
[33] V. Kamath, A. Prosperetti, F.N. Egolfopoulos, A theoretical study of sonoluminescence, J. Acoust. Soc. Am. 94 (1993) 248–260.
[34] S. Fujikawa, T. Akamatsu, Effects of the non-equilibrium condensation of vapour on the pressure wave produced by the collapse of a bubble in a liquid, J. Fluid Mech. 97 (1980) 481–512.
[35] K. Yasui, T. Tuziuti, Y. Iida, H. Mitome, Theoretical study of the ambient-pressure dependence of sonochemical reactions, J. Chem. Phys. 119 (2003) 346–356.
[36] K. Yasui, A new formulation of bubble dynamics for sonoluminescence (Ph.D. thesis), Waseda University, Japan, 1996.
[37] R. Toegel, D. Loshe, Phase diagrams for sonoluminescing bubbles, a comparison between experiment and theory, J. Chem. Phys. 118 (2003) 1863–1875.
[38] M.O. Conaire, H.J. Curran, J.M. Simmie, W.J. Pitz, C.K. Westbrook, A comprehensive modeling study of hydrogen oxidation, Int. J. Chem. Kinet. 36 (2004) 603–622.
[39] M.A. Mueller, T.J. Kim, R.A. Yetter, F.L. Dryer, Flow reactor studies and kinetic modeling of the H_2/O_2 reaction, Int. J. Chem. Kinet. 31 (1999) 113–125.
[40] K. Yasui, T. Tuziuti, M. Sivakumar, Y. Iida, Theoretical study of single bubble sonochemistry, J. Chem. Phys. 120 (2005) 224706-1–224706-12.

[41] G. Hauke, D. Fuster, C. Dopazo, Dynamic of a single cavitating and reacting bubble, Phys. Rev. E 75 (2007) 066310-1–066310-14.
[42] S. Labouret, J. Frohly, Distribution en tailles des bulles d'un champ de cavitation ultrasonore, 10ème Congrès Français d'Acoustique, Lyon, 2010. Available from: <http://hal.archives-ouvertes.fr/docs/00/55/11/51/PDF/000441.pdf>.
[43] K. Yasui, T. Tuziuti, J. Lee, T. Kozuka, A. Towada, The range of ambient radius for an active bubble in sonoluminescence and sonochemical reactions, J. Chem. Phys. 128 (2008) 184705-1–184705-12.
[44] J. Lee, M. Ashokkumar, S. Kentish, F. Grieser, Determination of the size distribution of sonoluminescence bubbles in a pulsed acoustic field, J. Am. Chem. Soc. 127 (2005) 16810–16811.
[45] W.-S. Chen, T.J. Matula, L.A. Crum, The disappearance of ultrasound contrast bubbles: observations of bubble dissolution and cavitation nucleation, Ultrasound Med. Biol. 28 (2002) 793–803.
[46] G. Mark, A. Tauber, R. Laupert, H.-P. Schechmann, D. Schulz, A. Mues, C. Von Sonntag, OH-radical formation by ultrasound in aqueous solution. Part II. Terephthalate and Fricke dosimetry and the influence of various conditions on the sonolytic yield, Utrason. Sonochem. 5 (1998) 41–52.
[47] Y.-Q. Gao, N.-Y. Gao, Y. Deng, J.-s. Gu, Y.-L. Gu, D. Zhang, Factor affecting sonolytic degradation of sulfamethazine in water, Ultrason. Sonochem. 20 (2013) 1401–1407.
[48] E.J. Hart, A. Henglein, Sonochemistry of aqueous solutions: H_2–O_2 combustion in cavitation bubbles, J. Phys. Chem. 91 (1987) 3654–3656.
[49] C.F. Beaton, G.F. Hewitt, Physical Property Data for the Design Engineer, Hemisphere Publishing Corporation, New York, 1989.
[50] K. Yasui, T. Tuziuti, Y. Iida, Optimum bubble temperature for the sonochemical production of oxidants, Ultrasonics 42 (2004) 579–584.
[51] P.G.T. Fogg, W. Gerrard, Solubility of Gases in Liquids, John Wiley & Sons Ltd., Chichester, UK, 1991.

Further reading

[21] S. Merouani, O. Hamdaoui, Y. Rezgui, M. Guemini, Theoretical procedure for the characterization of acoustic cavitation bubbles, Acta Acust. United Acust. (2014), accepted manuscript.